Euro. Jnl of Applied Mathematics (2012), *vol.* 23, *pp.* 635–657. © Cambridge University Press 2012
doi:10.1017/S0956792512000150

Numerical analysis of a piezoelectric bone remodelling problem

J. R. FERNÁNDEZ[1], J. M. GARCÍA-AZNAR[2] and R. MARTÍNEZ[3]

[1]*Departamento de Matemática Aplicada I, Universidade de Vigo, ETSI Telecomunicación, Campus As Lagoas Marcosende s/n, 36310 Vigo, Spain*
email: jose.fernandez@uvigo.es
[2]*Aragon Institute of Engineering Research (I3A), Universidad de Zaragoza, María de Luna, 3, E-50018, Zaragoza, Spain*
email: jmgaraz@unizar.es
[3]*Departamento de Matemática Aplicada, Universidade de Santiago de Compostela, Facultade de Matemáticas, Campus Sur s/n, 15782 Santiago de Compostela, Spain*
email: rebeca.martinez@usc.es

(*Received 22 July 2011; revised 30 April 2012; accepted 30 April 2012; first published online 25 May 2012*)

Although in recent years bone piezoelectricity has been normally neglected, lately a new interest has appeared to show the importance of bone piezoelectricity in wet bone's complex response to loading. Here we numerically study a problem, including a strain-adaptive bone remodelling and the piezoelectricity. Its variational formulation leads to a coupled system composed of two linear variational equations for displacements and electric potential, and a parabolic variational inequality for the apparent density. Fully discrete approximations are now introduced by using the finite element method to approximate spatial variable and the explicit Euler scheme to discretise time derivatives. Some *a priori* error estimates are proved and the linear convergence of the algorithm is deduced under additional regularity conditions. Finally, some one- and two-dimensional numerical simulations are described to show the accuracy of the proposed algorithm and the behaviour of the solution.

Key words: 65M15; 65M60; 74B20; 74F99

1 Introduction

Bone remodelling aims to understand the relationship between the morphology of the bone and the applied mechanical loads, and it is based on the fact that the bone has the ability to adapt itself to the load conditions which it is bearing. This adaptation process, including modelling and remodelling mechanisms, has an enormous effect on the overall behaviour and health of the entire body. For instance, it is well argued that normal and daily activities generate damage in the form of tiny microcracks throughtout bone tissue.

Since the first mathematical analysis of a bone remodelling model presented in [10,21], several papers have been published; most of them are based on the qualitative observations provided by Wolff in [51] (see, e.g. [14]). In this paper we use the bone remodelling model introduced in [49], which is based on the principle that bone remodelling is induced by a local mechanical signal that activates the regulating bone cells; i.e. they consider that the bone has sensors that can detect a mechanical stimulus, and, depending on its magnitude,

https://doi.org/10.1017/S0956792512000150 Published online by Cambridge University Press

cause local bone adaptations. The main idea of this model is to use the apparent density as an internal variable able to characterise internal morphology.

Piezoelectricity is the ability of certain materials, like quartz (also ceramics ($BaTiO_3$, $KNbO_3$, $LiNbO_3$, PZT-5A etc) and even human bones like the mandible), to produce a voltage when they are subjected to mechanical stress (see, for instance, [25, 30–35, 36, 43–46]. The piezoeletric effect is characterised by the coupling between the mechanical and electrical properties of the material: It was observed that the appearance of electric charges on some crystals was due to the action of body forces and surface tractions (the so-called indirect or sensor effect) and, conversely, the action of the electric field-generated strain or stress in the body (the so-called direct or actuator effect). Observations show that the human bone has electrical and dielectrical properties depending on the frequency (see [40, 41]). In fact, as it was noticed in [39], electrical properties of bone are relevant not only as an hypothesised feedback mechanism for bone adaptation and remodelling but also in the context of external electrical stimulation of bone in order to aid its healing and repair.

Recently, there has been great interest (see [26]) in understanding the piezoelectric behaviour of bone and its impact in bone remodelling. Fukada and Yasuda (see [15, 16]) have first demonstrated that dry bone is piezoelectric in the above classical sense. Since then many authors have confirmed the capacity of bones to produce piezoelectric potentials (see, e.g., [2, 3, 17, 19, 28]). During the last thirty years, many attempts have been made to study the coupling between the bone remodelling and the piezoelectric effect (see, e.g., [7, 13, 19, 27, 29, 37–42, 47]). However, despite these numerous models, the exact relationship between the two phenomena is still unknown. Moreover, in recent years piezoelectric strain-adaptive bone remodelling model has been neglected. In fact, it has been considered that in living, or wet, bone these piezoelectric effects are very minor and dominated by electrokinetic effects, streaming currents and zeta potentials. However, recent works (see [1, 26]) review the role of bone piezoelectricity (mainly based on collagen) as a mediator for bone regulation in bone remodelling, healing and growth. In most of the above-mentioned works, the authors used, in order to simplify calculations, a simpler bone remodelling law introduced in Cowin and Hegedus [10] (also described in detail in the review paper [9]). In this paper we consider the more complicated, and more interesting from the biomechanical point of view, bone remodelling law introduced in Weinans *et al.* [49] and, according to the above-mentioned papers, we assume an electro-mechanical dependence for mechanical properties. A similar approach has been also used for the modelling of damaged piezoelectric ceramic materials (see [50]). Fully discrete approximations are proposed, error estimates are proved and some numerical simulations are presented to demonstrate the convergence of algorithm and behaviour of the solution.

The paper is outlined as follows. In Section 2 we briefly describe the mechanical problem and derive its variational formulation. Then, a fully discrete scheme, based on the finite element method to approximate the spatial variable and the Euler scheme to discretise time derivatives, is introduced in Section 3. A main error estimates' result is proved from which, under suitable regularity conditions, the linear convergence of the algorithm is deduced. In Section 4, a numerical algorithm to solve a fully discrete problem is described, a one-dimensional (1D) numerical simulation is performed to show the

https://doi.org/10.1017/S0956792512000150 Published online by Cambridge University Press

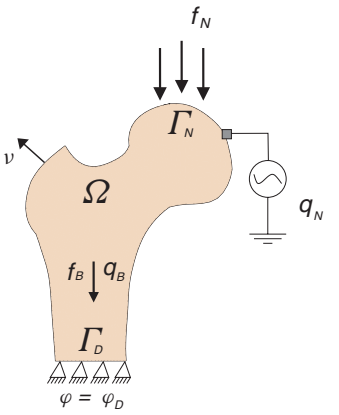


FIGURE 1. (Colour online) A piezoelectric bone remodelling problem.

accuracy of the finite element approximation and, finally, some 2D numerical simulations are presented to demonstrate the behaviour of the solution.

2 The mechanical problem and its variational formulation

Let $\Omega \subset \mathbb{R}^d$, $d = 1, 2, 3$, be an open-bounded domain and denote by $\Gamma = \partial\Omega$ its boundary, which is assumed to be the Lipschitz continuous and divided into two disjoint parts Γ_D and Γ_N. Let $[0, T]$, $T > 0$, be the time interval of interest, denoted by $\boldsymbol{x} = (x_i)_{i=1}^d$ a generic point of $\overline{\Omega} = \Omega \cup \Gamma$, and, for $\boldsymbol{x} \in \Gamma$, let $\boldsymbol{\nu}(\boldsymbol{x}) = (\nu_i(\boldsymbol{x}))_{i=1}^d$ be the outward unit normal vector to Γ at point $\boldsymbol{x}$. Volume forces of density $\boldsymbol{f}_B$ are supposed to act in $\Omega \times (0, T)$, volume electric charges of density q_B are present in $\Omega \times (0, T)$, traction forces of density $\boldsymbol{f}_N$ are applied on $\Gamma_N \times (0, T)$ and surface electric charges of density q_N are found on $\Gamma_N \times (0, T)$. Finally, we assume that the body is clamped on $\Gamma_D \times (0, T)$ (i.e. $\boldsymbol{u} = \boldsymbol{0}$) and a prescribed electric potential φ_D is applied there (see Figure 1).

Remark 1 Notice that we have used the same decomposition of the boundary to impose the boundary conditions for the displacements and the electric potential. It is straightforward to extend the results presented in this section, and in the following one, to more general situations.

Let φ, $\boldsymbol{u} = (u_i)_{i=1}^d$, $\boldsymbol{\sigma} = (\sigma_{ij})_{i,j=1}^d$ and $\boldsymbol{\varepsilon}(\boldsymbol{u}) = (\varepsilon_{ij}(\boldsymbol{u}))_{i,j=1}^d$ be the electric potential, the displacement field, the stress field and the linearised strain tensor, respectively.

As a first approach and according to [49, 50], the bone is assumed to be linear, elastic and isotropic, and the constitutive law is written in the following form:

$$\boldsymbol{\sigma} = 2\,\mu(\rho)\boldsymbol{\varepsilon}(\boldsymbol{u}) + \lambda(\rho)\mathrm{Div}\,(\boldsymbol{u})\mathcal{I} - \alpha(\rho)\mathcal{E}^*\mathbf{E}(\varphi) \quad \text{in} \quad \overline{\Omega} \times [0, T],$$

where $\alpha(\rho)$ is a constitutive function described below, $\mathbf{E}(\varphi) = (E_i(\varphi))_{i=1}^d$ represents the electric field defined by

$$E_i(\varphi) = -\frac{\partial\varphi}{\partial x_i}, \quad i = 1, \ldots, d,$$

https://doi.org/10.1017/S0956792512000150 Published online by Cambridge University Press

and $\mathscr{E}^* = (e^*_{ijk})^d_{i,j,k=1}$ denotes the transpose of the third-order piezoelectric tensor $\mathscr{E} = (e_{ijk})^d_{i,j,k=1}$. We recall that

$$e^*_{ijk} = e_{kij}, \quad \text{for all} \quad i,j,k = 1,\ldots,d.$$

Moreover, $\mathscr{I}$ denotes the identity operator in the space of the second-order symmetric tensors $\mathbb{S}^d$, Div represents the divergence operator and $\mu(\rho)$ and $\lambda(\rho)$ are Lamé's coefficients of the material, assumed to depend on the apparent density of the bone denoted by ρ. These coefficients can also be given as a function of Young's modulus $E(\rho)$ and Poisson's ratio $\kappa(\rho)$ by

$$\mu(\rho) = \frac{E(\rho)}{2(1+\kappa(\rho))}, \quad \lambda(\rho) = \frac{\kappa(\rho)E(\rho)}{1-\kappa^2(\rho)}$$

if the plane stress hypothesis is assumed, or

$$\mu(\rho) = \frac{E(\rho)}{2(1+\kappa(\rho))}, \quad \lambda(\rho) = \frac{\kappa(\rho)E(\rho)}{(1+\kappa(\rho))(1-2\kappa(\rho))}$$

if the plane strain hypothesis is used or the 3D case is considered. Moreover, we also assume that Poisson's ratio is independent of the apparent density (and so, $\kappa(\rho) = \kappa$), and, according to [49], the following equation is used for Young's modulus depending on apparent density:

$$E(\rho) = M\rho^\gamma,$$

where M, $\gamma > 0$ are constitutive constants.

Following [6,22,24,48,49] we assume that the rate of bone remodelling is regulated by a mechanical-based stimulus and it is written as follows:

$$\dot{\rho} = B\left(\frac{\boldsymbol{\sigma} : \boldsymbol{\varepsilon}(\boldsymbol{u})}{2\rho} - S_r\right) \quad \text{in} \quad \Omega \times (0,T), \quad \rho_a \leqslant \rho \leqslant \rho_b,$$

where B and S_r are experimental constants, and ρ_a and ρ_b represent the minimal density corresponding to the reabsorbed bone and the maximal density of the cortical bone, respectively.

According to [5,50] the following constitutive law is employed for electric potential,

$$\mathbf{D} = \alpha(\rho)\mathscr{E}\boldsymbol{\varepsilon}(\boldsymbol{u}) + \alpha(\rho)\beta\mathbf{E}(\varphi),$$

where $\mathbf{D}$ is the electric displacement field, β is the electric permittivity tensor and $\alpha(\rho)$ is a constitutive function, which states the dependence on the apparent density function. No experimental studies are known about its form and so here, in order to simplify writing and calculations, we assume that

$$\alpha(\rho) = \rho^\gamma.$$

We note that this choice of function $\alpha(\rho)$ is just an example and it is based on similar dependence for Young's modulus.

https://doi.org/10.1017/S0956792512000150 Published online by Cambridge University Press

Let ρ_0 be the initial apparent density. Assuming that the process is quasistatic and using the continuous mechanics law in the framework of small displacements theory, the deformation of a piezoelectric bone can be obtained as follows.

Problem P. Find a displacement field $\boldsymbol{u} : \overline{\Omega} \times [0,T] \to \mathbb{R}^d$, an stress field $\boldsymbol{\sigma} : \overline{\Omega} \times [0,T] \to \mathbb{S}^d$, an electric potential field $\varphi : \overline{\Omega} \times (0,T) \to \mathbb{R}$, an electric displacement field $\mathbf{D} : \overline{\Omega} \times (0,T) \to \mathbb{R}^d$ and an apparent density function $\rho : \overline{\Omega} \times [0,T] \to [\rho_a, \rho_b]$ such that $\rho(0) = \rho_0$ and,

$$\dot{\rho} = B\left(\frac{U(\boldsymbol{\sigma}, \boldsymbol{\varepsilon}(\boldsymbol{u}))}{\rho} - S_r\right) \quad \text{in} \quad \Omega \times (0,T), \tag{2.1}$$

$$\boldsymbol{\sigma} = 2\mu(\rho)\boldsymbol{\varepsilon}(\boldsymbol{u}) + \lambda(\rho)\mathrm{Div}\,(\boldsymbol{u})\mathcal{I} - \rho^\gamma \mathcal{E}^* \mathbf{E}(\varphi) \quad \text{in} \quad \Omega \times [0,T], \tag{2.2}$$

$$\mathbf{D} = \rho^\gamma \mathcal{E}\boldsymbol{\varepsilon}(\boldsymbol{u}) + \rho^\gamma \beta \mathbf{E}(\varphi) \quad \text{in} \quad \Omega \times (0,T), \tag{2.3}$$

$$-\mathrm{Div}\,\boldsymbol{\sigma} = \boldsymbol{f}_B \quad \text{in} \quad \Omega \times (0,T), \tag{2.4}$$

$$\mathrm{div}\,\mathbf{D} = q_B \quad \text{in} \quad \Omega \times (0,T), \tag{2.5}$$

$$\boldsymbol{u} = \mathbf{0} \quad \text{on} \quad \Gamma_D \times (0,T), \tag{2.6}$$

$$\varphi = \varphi_D \quad \text{on} \quad \Gamma_D \times (0,T), \tag{2.7}$$

$$\boldsymbol{\sigma}\boldsymbol{v} = \boldsymbol{f}_N \quad \text{on} \quad \Gamma_N \times (0,T), \tag{2.8}$$

$$\mathbf{D} \cdot \boldsymbol{v} = q_N \quad \text{on} \quad \Gamma_N \times (0,T), \tag{2.9}$$

where Lamé's coefficients $\lambda(\rho)$ and $\mu(\rho)$ were defined above.

Let us now obtain a variational formulation of the above mechanical problem. Denote by $Y = L^2(\Omega)$ and $H = [L^2(\Omega)]^d$, and define the following variational spaces for electric potential, displacements and stresses:

$$\begin{aligned} W &= \{\psi \in H^1(\Omega) \ ; \ \psi = 0 \quad \text{on} \quad \Gamma_D\}, \\ V &= \{\boldsymbol{v} = (v_i)_{i=1}^d \in [H^1(\Omega)]^d \ ; \ \boldsymbol{v} = \mathbf{0} \quad \text{on} \quad \Gamma_D\}, \\ Q &= \{\boldsymbol{\tau} = (\tau_{ij})_{i,j=1}^d \in [L^2(\Omega)]^{d\times d} \ ; \ \tau_{ij} = \tau_{ji}, \quad 1 \leqslant i,j \leqslant d\}, \end{aligned}$$

and the discrete convex set of admissible apparent density functions:

$$K = \{\xi \in Y \ ; \ \rho_a \leqslant \xi \leqslant \rho_b, \ \text{a.e. in } \Omega\}.$$

In order to obtain the variational formulation of Problem P and to prove the *a priori* error estimates of the next section, we have to make the following assumptions.

(i) The density of mechanical and electrical forces have the regularity:

$$\begin{aligned} &\boldsymbol{f}_B \in C([0,T]; [C(\overline{\Omega})]^d), \quad \boldsymbol{f}_N \in C([0,T]; [C(\overline{\Gamma}_N)]^d), \\ &q_B \in C([0,T]; C(\overline{\Omega})), \quad q_N \in C([0,T]; C(\overline{\Gamma}_N)). \end{aligned} \tag{2.10}$$

(ii) The initial apparent density ρ_0 satisfies the following conditions:

$$\rho_0 \in C(\overline{\Omega}), \quad \rho_a \leqslant \rho_0(\boldsymbol{x}) \leqslant \rho_b \quad \text{for all} \quad \boldsymbol{x} \in \overline{\Omega}. \tag{2.11}$$

https://doi.org/10.1017/S0956792512000150 Published online by Cambridge University Press

(iii) The piezoelectric tensor $\mathscr{E}(\boldsymbol{x}) = (e_{ijk}(\boldsymbol{x}))_{i,j,k=1}^{d} : \boldsymbol{\tau} \in \mathbb{S}^d \to \mathscr{E}(\boldsymbol{x})(\boldsymbol{\tau}) \in \mathbb{R}^d$ satisfies

$$\begin{aligned} &\text{(a) } e_{ijk} = e_{ikj} \quad \text{for} \quad i,j,k = 1,\dots,d. \\ &\text{(b) } e_{ijk} \in L^\infty(\Omega) \quad \text{for} \quad i,j,k = 1,\dots,d. \end{aligned} \tag{2.12}$$

(iv) The permittivity tensor $\beta(\boldsymbol{x}) = (\beta_{ij}(\boldsymbol{x}))_{i,j=1}^{d} : \boldsymbol{w} \in \mathbb{R}^d \to \beta(\boldsymbol{x})(\boldsymbol{w}) \in \mathbb{R}^d$ satisfies

$$\begin{aligned} &\text{(a) } \beta_{ij} = \beta_{ji} \quad \text{for} \quad i,j = 1,\dots,d. \\ &\text{(b) } \beta_{ij} \in L^\infty(\Omega) \quad \text{for} \quad i,j = 1,\dots,d. \\ &\text{(c) There exists } m_\beta > 0 \text{ such that } \beta(\boldsymbol{x})\boldsymbol{w}\cdot\boldsymbol{w} \geqslant m_\beta\,|\boldsymbol{w}|^2 \\ &\qquad \forall\, \boldsymbol{w} \in \mathbb{R}^d, \text{ a.e. } \boldsymbol{x} \in \Omega. \end{aligned} \tag{2.13}$$

In order to simplify the writing, for every $\rho \in L^\infty(\Omega)$ we define the bilinear form $c(\rho;\cdot,\cdot) : V \times V \to \mathbb{R}$ as

$$c(\rho;\boldsymbol{u},\boldsymbol{v}) = \int_\Omega 2\mu(\rho)\boldsymbol{\varepsilon}(\boldsymbol{u}) \,:\boldsymbol{\varepsilon}(\boldsymbol{v}) + \lambda(\rho)\mathrm{Tr}(\boldsymbol{\varepsilon}(\boldsymbol{u}))\mathrm{Tr}(\boldsymbol{\varepsilon}(\boldsymbol{v}))\,d\boldsymbol{x}, \quad \forall \boldsymbol{u},\, \boldsymbol{v} \in V,$$

where Tr denotes the classical trace operator.

Moreover, using the Riesz theorem, we define the linear mappings $\boldsymbol{f} : [0,T] \to V$ and $q : [0,T] \to W$ given by

$$\begin{aligned} (\boldsymbol{f}(t),\boldsymbol{v})_V &= \int_\Omega \boldsymbol{f}_B(t)\cdot\boldsymbol{v}\,d\boldsymbol{x} + \int_{\Gamma_N} \boldsymbol{f}_N(t)\cdot\boldsymbol{v}\,d\Gamma \quad \forall \boldsymbol{v} \in V, \\ (q(t),\boldsymbol{v})_W &= \int_\Omega q_B(t)\psi\,d\boldsymbol{x} + \int_{\Gamma_N} q_N(t)\psi\,d\Gamma \quad \forall \psi \in W. \end{aligned}$$

In order to derive the weak form of equation (2.1), according to [11] we introduce the function

$$\Phi(\rho,\boldsymbol{\sigma},\boldsymbol{\tau}) = B\left(\frac{\boldsymbol{\sigma} \,:\mathscr{L}(\boldsymbol{\tau})}{2\rho} - S_r\right), \tag{2.14}$$

where $\mathscr{L} : \mathbb{S}^d \to \mathbb{S}^d$ is the truncation operator given by

$$(\mathscr{L}(\boldsymbol{\tau}))_{ij} = \begin{cases} L & \text{if} \quad \tau_{ij} > L, \\ \tau_{ij} & \text{if} \quad \tau_{ij} \in [-L,L], \\ -L & \text{if} \quad \tau_{ij} < -L. \end{cases}$$

Therefore, equation (2.1) is equivalent to the following parabolic differential inclusion:

$$\dot{\rho} - \Phi(\rho,\boldsymbol{\sigma},\boldsymbol{\tau}) + \partial I_{[\rho_a,\rho_b]}(\rho) \ni 0.$$

Here, $\partial I_{[\rho_a,\rho_b]}$ denotes the sub-differential of the indicator function of the interval $[\rho_a,\rho_b]$.

Finally, in order to simplify the calculations and the writing, we assume in this section, and also in the following one, that $\varphi_D = 0$.

Applying Green's formula, we obtain the following variational formulation.

Problem VP. Find a displacement field $\boldsymbol{u} : [0,T] \to V$, an electric potential field $\varphi : [0,T] \to W$ and an apparent density function $\rho : [0,T] \to K$ such that $\rho(0) = \rho_0$ and for

https://doi.org/10.1017/S0956792512000150 Published online by Cambridge University Press

a.e. $t \in (0, T)$,

$$c(\rho(t); \boldsymbol{u}(t), \boldsymbol{v}) = (\boldsymbol{f}(t), \boldsymbol{v})_V - (\rho(t)^\gamma \mathscr{E}^* \nabla\varphi(t), \boldsymbol{\varepsilon}(\boldsymbol{v}))_Q \quad \forall \boldsymbol{v} \in V, \tag{2.15}$$

$$(\rho(t)^\gamma [\beta \nabla\varphi(t) - \mathscr{E}\boldsymbol{\varepsilon}(\boldsymbol{u}(t))], \nabla\psi)_H = (q(t), \psi)_W \quad \forall \psi \in W, \tag{2.16}$$

$$(\dot{\rho}(t), \xi - \rho(t))_Y \geqslant (\Phi(\rho(t), \boldsymbol{\sigma}(t), \boldsymbol{\varepsilon}(\boldsymbol{u}(t))), \xi - \rho(t))_Y \quad \forall \xi \in K. \tag{2.17}$$

Owing to the absence of the diffusion term in the parabolic variational inequality (2.17), the existence of a unique solution to the above variational problem remains an open problem yet. This is because the arguments used in the study of damage problems cannot be applied here (see, for instance, [12]).

3 Fully discrete scheme: *a priori* error estimates

The fully discrete approximation of Problem VP is done as follows. First, the spatial variable is approximated assuming that $\overline{\Omega}$ is a polyhedral domain and denoting by $\mathscr{T}^h$ a triangulation of $\overline{\Omega}$, compatible with the partition of the boundary $\Gamma = \partial\Omega$ into Γ_D and Γ_N. Here, $h > 0$ represents the spatial discretisation parameter. Then we define the finite element spaces:

$$V^h = \{\boldsymbol{v}^h \in [C(\overline{\Omega})]^d \ ; \ \boldsymbol{v}^h_{|_T} \in [P_1(T)]^d, \ T \in \mathscr{T}^h, \quad \boldsymbol{v}^h = \boldsymbol{0} \ \text{ on } \ \Gamma_D\}, \tag{3.1}$$

$$Q^h = \{\boldsymbol{\tau}^h \in [L^2(\Omega)]^{d\times d} \ ; \ \boldsymbol{\tau}^h_{|_T} \in [P_0(T)]^{d\times d}, \ T \in \mathscr{T}^h\}, \tag{3.2}$$

$$W^h = \{\psi^h \in C(\overline{\Omega}) \ ; \ \psi^h_{|_T} \in P_1(T), \ T \in \mathscr{T}^h, \quad \psi^h = 0 \ \text{ on } \ \Gamma_D\}, \tag{3.3}$$

$$B^h = \{\xi^h \in Y \ ; \ \xi^h_{|_T} \in P_0(T), \quad T \in \mathscr{T}^h\}, \tag{3.4}$$

and the discrete convex set of admissible apparent density functions:

$$K^h = \{\xi^h \in B^h \ ; \ \rho_a \leqslant \xi^h \leqslant \rho_b \quad \text{in} \quad \Omega\}, \tag{3.5}$$

where $P_q(T)$, $q = 0, 1$, represents the space of polynomials of global degree less or equal to q in T.

Secondly, we discretise the time derivatives by using a uniform partition of the time interval $[0, T]$, defined by $0 = t_0 < t_1 < \ldots < t_N = T$, and we denote by k the time step size, $k = T/N$. Moreover, for a continuous function $f(t)$ let $f_n = f(t_n)$.

Therefore, using the forward Euler scheme, we obtain the following fully discrete approximation of Problem VP.

Problem VP^{hk} Find a discrete displacement field $\boldsymbol{u}^{hk} = \{\boldsymbol{u}^{hk}_n\}_{n=0}^N \subset V^h$, a discrete electric potential field $\varphi^{hk} = \{\varphi^{hk}_n\}_{n=0}^N \subset W^h$ and a discrete apparent density function

https://doi.org/10.1017/S0956792512000150 Published online by Cambridge University Press

$\rho^{hk} = \{\rho_n^{hk}\}_{n=0}^N \subset K^h$ such that for all $\boldsymbol{v}^h \in V^h$, $\psi^h \in W^h$ and $\xi^h \in K^h$,

$$c(\rho_n^{hk}; \boldsymbol{u}_n^{hk}, \boldsymbol{v}^h) = (\boldsymbol{f}_n, \boldsymbol{v}^h)_V - ((\rho_n^{hk})^\gamma \mathscr{E}^* \nabla\varphi_n^{hk}, \boldsymbol{\varepsilon}(\boldsymbol{v}^h))_Q, \ n = 0, 1, \ldots, N, \tag{3.6}$$

$$((\rho_n^{hk})^\gamma [\beta \nabla\varphi_n^{hk} - \mathscr{E}\boldsymbol{\varepsilon}(\boldsymbol{u}_n^{hk})], \nabla\psi^h)_H = (q_n, \psi^h)_W, \quad n = 0, 1, \ldots, N, \tag{3.7}$$

$$\left(\frac{\rho_n^{hk} - \rho_{n-1}^{hk}}{k}, \xi^h - \rho_n^{hk}\right)_Y \geqslant \left(\Phi(\rho_{n-1}^{hk}, \boldsymbol{\sigma}_{n-1}^{hk}, \boldsymbol{\varepsilon}(\boldsymbol{u}_{n-1}^{hk})), \xi^h - \rho_n^{hk}\right)_Y, \quad n = 1, 2, \ldots, N. \tag{3.8}$$

Here the discrete stress field $\boldsymbol{\sigma}^{hk} = (\boldsymbol{\sigma}_n^{hk})_{n=0}^N \subset Q^h$ has the following form:

$$\boldsymbol{\sigma}_n^{hk} = 2\,\mu(\rho_n^{hk})\boldsymbol{\varepsilon}(\boldsymbol{u}_n^{hk}) + \lambda(\rho_n^{hk})\mathrm{Div}\,(\boldsymbol{u}_n^{hk})\mathscr{I} + (\rho_n^{hk})^\gamma \mathscr{E}^* \nabla\varphi_n^{hk}, \quad n = 0, 1, \ldots, N, \tag{3.9}$$

and ρ_0^{hk} denotes an appropriate approximation of the initial condition ρ_0.

The existence of a unique discrete solution to Problem VP^{hk} can be easily proved by using classical results on linear variational inequalities (see [18]).

Now we will derive some *a priori* error estimates. Therefore, we need to assume the following additional regularity conditions:

$$\begin{aligned} &\boldsymbol{u} \in C^1([0, T]; V) \cap C([0, T]; [W^{1,\infty}(\overline{\Omega})]^d), \quad \rho \in C^1([0, T]; Y), \\ &\varphi \in C^1([0, T]; W) \cap C([0, T]; W^{1,\infty}(\overline{\Omega})). \end{aligned} \tag{3.10}$$

First, error estimates for the apparent density functions were already derived in [11] for the case without piezoelectric effects. Proceeding in an analogous way, the following estimates are proved for all $\{\xi_j^h\}_{j=1}^n \subset K^h$:

$$\begin{aligned} \|\rho_n - \rho_n^{hk}\|_Y^2 &\leqslant Ck \sum_{j=1}^n \Big\{ \|\boldsymbol{u}_j - \boldsymbol{u}_j^{hk}\|_V^2 + \|\rho_j - \rho_j^{hk}\|_Y^2 + \|\rho_j - \xi_j^h\|_Y^2 + \|\varphi_j - \varphi_j^{hk}\|_W^2 \\ &\quad + \left\|\Phi_j - \frac{\rho_j - \rho_{j-1}}{k}\right\|_Y \|\rho_j - \xi_j^h\|_Y + \|\rho_j - \rho_{j-1}\|_Y^2 \\ &\quad + \|\boldsymbol{u}_j - \boldsymbol{u}_{j-1}\|_V^2 + \|\varphi_j - \varphi_{j-1}\|_W^2 + \left\|\frac{\rho_j - \rho_{j-1}}{k} - \dot{\rho}_j\right\|_Y^2 \Big\} \\ &\quad + \frac{C}{k} \sum_{j=1}^{n-1} \|\rho_j - \xi_j^h - (\rho_{j+1} - \xi_{j+1}^h)\|_Y^2 + C\|\rho_1 - \xi_1^h\|_Y^2 + C\|\rho_n - \xi_n^h\|_Y^2 \\ &\quad + C\|\rho_0 - \rho_0^{hk}\|_Y^2 + C\|\boldsymbol{u}_0 - \boldsymbol{u}_0^{hk}\|_V^2 + C\|\varphi_0 - \varphi_0^{hk}\|_W^2, \end{aligned} \tag{3.11}$$

where we used the notation $\Phi_j = \Phi(\rho_j, \boldsymbol{\sigma}(\boldsymbol{u}_j), \boldsymbol{\varepsilon}(\boldsymbol{u}_j))$ and, here and in what follows, C denotes a generic positive constant which depends on the continuous solution but it is independent of discretisation parameters h and k. Moreover, we note that these error estimates depend on the electric potential because the stress field does it too.

Secondly, we turn to estimate numerical errors on the electric potential and the displacement field simultaneously. Hence, subtracting variational equation (2.16) at time $t = t_n$

https://doi.org/10.1017/S0956792512000150 Published online by Cambridge University Press

for $\psi = \psi^h \in W^h$ and variational equation (3.7) we find that

$$(\rho_n^\gamma[\beta\nabla\varphi_n - \mathscr{E}\boldsymbol{\varepsilon}(\boldsymbol{u}_n)] - (\rho_n^{hk})^\gamma[\beta\nabla\varphi_n^{hk} - \mathscr{E}\boldsymbol{\varepsilon}(\boldsymbol{u}_n^{hk})], \nabla\psi^h)_H = 0,$$

and therefore,

$$\begin{aligned}(\rho_n^\gamma[\beta\nabla\varphi_n - \mathscr{E}\boldsymbol{\varepsilon}(\boldsymbol{u}_n)] - (\rho_n^{hk})^\gamma[\beta\nabla\varphi_n^{hk} - \mathscr{E}\boldsymbol{\varepsilon}(\boldsymbol{u}_n^{hk})], \nabla(\varphi_n - \varphi_n^{hk}))_H \\ = (\rho_n^\gamma[\beta\nabla\varphi_n - \mathscr{E}\boldsymbol{\varepsilon}(\boldsymbol{u}_n)] - (\rho_n^{hk})^\gamma[\beta\nabla\varphi_n^{hk} - \mathscr{E}\boldsymbol{\varepsilon}(\boldsymbol{u}_n^{hk})], \nabla(\varphi_n - \psi^h))_H\end{aligned}$$

for all $\psi^h \in W^h$.

Taking into account that

$$\begin{aligned}(\rho_n^\gamma[\beta\nabla\varphi_n - \mathscr{E}\boldsymbol{\varepsilon}(\boldsymbol{u}_n)] - (\rho_n^{hk})^\gamma[\beta\nabla\varphi_n^{hk} - \mathscr{E}\boldsymbol{\varepsilon}(\boldsymbol{u}_n^{hk})], \nabla\psi)_H \\ = ((\rho_n^{hk})^\gamma[\beta\nabla(\varphi_n - \varphi_n^{hk}) - \mathscr{E}\boldsymbol{\varepsilon}(\boldsymbol{u}_n - \boldsymbol{u}_n^{hk})], \nabla\psi)_H \\ + ((\rho_n^\gamma - (\rho_n^{hk})^\gamma)[\beta\nabla\varphi_n - \mathscr{E}\boldsymbol{\varepsilon}(\boldsymbol{u}_n)], \nabla\psi)_H \quad \forall\psi \in W,\end{aligned}$$

we have

$$\begin{aligned}-((\rho_n^{hk})^\gamma\mathscr{E}\boldsymbol{\varepsilon}(\boldsymbol{u}_n - \boldsymbol{u}_n^{hk}), \nabla(\varphi_n - \varphi_n^{hk}))_H \\ = ((\rho_n^\gamma - (\rho_n^{hk})^\gamma)\mathscr{E}\boldsymbol{\varepsilon}(\boldsymbol{u}_n), \nabla(\varphi_n - \varphi_n^{hk}))_H \\ - ((\rho_n^\gamma - (\rho_n^{hk})^\gamma)\beta\nabla\varphi_n, \nabla(\varphi_n - \varphi_n^{hk}))_H \\ - ((\rho_n^{hk})^\gamma\nabla(\varphi_n - \varphi_n^{hk}), \nabla(\varphi_n - \varphi_n^{hk}))_H \\ + ((\rho_n^{hk})^\gamma\beta\nabla(\varphi_n - \varphi_n^{hk}), \nabla(\varphi_n - \psi^h))_H \\ + ((\rho_n^\gamma - (\rho_n^{hk})^\gamma\beta\nabla\varphi_n, \nabla(\varphi_n - \psi^h))_H \\ - ((\rho_n^{hk})^\gamma\mathscr{E}\boldsymbol{\varepsilon}(\boldsymbol{u}_n - \boldsymbol{u}_n^{hk}), \nabla(\varphi_n - \psi^h))_H \\ - ((\rho_n^\gamma - (\rho_n^{hk})^\gamma)\mathscr{E}\boldsymbol{\varepsilon}(\boldsymbol{u}_n), \nabla(\varphi_n - \psi^h))_H \quad \forall\psi^h \in W^h. \qquad (3.12)\end{aligned}$$

Next, subtracting variational equation (2.15) at time $t = t_n$ for $\boldsymbol{v} = \boldsymbol{v}^h \in V^h$ and variational equation (3.6) we find that

$$c(\rho_n; \boldsymbol{u}_n, \boldsymbol{v}^h) - c(\rho_n^{hk}; \boldsymbol{u}_n^{hk}, \boldsymbol{v}^h) + (\rho_n^\gamma\mathscr{E}^*\nabla\varphi_n - (\rho_n^{hk})^\gamma\mathscr{E}^*\nabla\varphi_n^{hk}, \boldsymbol{\varepsilon}(\boldsymbol{v}^h))_Q = 0,$$

for all $\boldsymbol{v}^h \in V^h$. Therefore,

$$\begin{aligned}c(\rho_n; \boldsymbol{u}_n, \boldsymbol{u}_n - \boldsymbol{u}_n^{hk}) - c(\rho_n^{hk}; \boldsymbol{u}_n^{hk}, \boldsymbol{u}_n - \boldsymbol{u}_n^{hk}) \\ + (\rho_n^\gamma\mathscr{E}^*\nabla\varphi_n - (\rho_n^{hk})^\gamma\mathscr{E}^*\nabla\varphi_n^{hk}, \boldsymbol{\varepsilon}(\boldsymbol{u}_n - \boldsymbol{u}_n^{hk}))_Q \\ = c(\rho_n; \boldsymbol{u}_n, \boldsymbol{u}_n - \boldsymbol{v}^h) - c(\rho_n^{hk}; \boldsymbol{u}_n^{hk}, \boldsymbol{u}_n - \boldsymbol{v}^h) \\ + (\rho_n^\gamma\mathscr{E}^*\nabla\varphi_n - (\rho_n^{hk})^\gamma\mathscr{E}^*\nabla\varphi_n^{hk}, \boldsymbol{\varepsilon}(\boldsymbol{u}_n - \boldsymbol{v}^h))_Q \quad \forall\boldsymbol{v}^h \in V^h.\end{aligned}$$

From the regularity $\boldsymbol{u} \in C([0,T]; [W^{1,\infty}(\overline{\Omega})]^{d\times d})$ (which implies that $\boldsymbol{\varepsilon}(\boldsymbol{u}_n) \in [L^\infty(\overline{\Omega})]^{d\times d}$) and keeping in mind that the apparent density functions $\rho_n, \rho_n^{hk} \in [\rho_a, \rho_b]$, after easy algebraic manipulations it follows that

$$\begin{aligned}&c(\rho_n; \boldsymbol{u}_n, \boldsymbol{u}_n - \boldsymbol{u}_n^{hk}) - c(\rho_n^{hk}; \boldsymbol{u}_n, \boldsymbol{u}_n - \boldsymbol{u}_n^{hk}) \leqslant C\|\rho_n - \rho_n^{hk}\|_Y\|\boldsymbol{u}_n - \boldsymbol{u}_n^{hk}\|_V, \\ &c(\rho_n; \boldsymbol{u}_n, \boldsymbol{u}_n - \boldsymbol{v}^h) - c(\rho_n^{hk}; \boldsymbol{u}_n^{hk}, \boldsymbol{u}_n - \boldsymbol{v}^h) \\ &\quad \leqslant C\|\boldsymbol{u}_n - \boldsymbol{u}_n^{hk}\|_V\|\boldsymbol{u}_n - \boldsymbol{v}^h\|_V + C\|\rho_n - \rho_n^{hk}\|_Y\|\boldsymbol{u}_n - \boldsymbol{v}^h\|_V.\end{aligned}$$

https://doi.org/10.1017/S0956792512000150 Published online by Cambridge University Press

By using properties (iii)–(iv) and equation (3.12), taking into account that $\rho_n, \rho_n^{hk} \in [\rho_a, \rho_b]$, the equations

$$
\begin{aligned}
&(\rho_n^{\gamma}\mathscr{E}^*\nabla\varphi_n - (\rho_n^{hk})^{\gamma}\mathscr{E}^*\nabla\varphi_n^{hk}, \boldsymbol{\varepsilon}(\boldsymbol{v}))_Q = ((\rho_n^{hk})^{\gamma}\mathscr{E}^*\nabla(\varphi_n - \varphi_n^{hk}), \boldsymbol{\varepsilon}(\boldsymbol{v}))_Q \\
&\quad + ((\rho_n^{\gamma} - (\rho_n^{hk})^{\gamma})\mathscr{E}^*\nabla\varphi_n, \boldsymbol{\varepsilon}(\boldsymbol{v}))_Q \quad \forall \boldsymbol{v} \in V, \\
&((\rho_n^{hk})^{\gamma}\mathscr{E}^*\nabla(\varphi_n - \varphi_n^{hk}), \boldsymbol{\varepsilon}(\boldsymbol{u}_n - \boldsymbol{u}_n^{hk}))_Q = ((\rho_n^{hk})^{\gamma}\mathscr{E}\boldsymbol{\varepsilon}(\boldsymbol{u}_n - \boldsymbol{u}_n^{hk}), \nabla(\varphi_n - \varphi_n^{hk}))_H, \\
&c(\rho_n^{hk}; \boldsymbol{u}_n, \boldsymbol{u}_n - \boldsymbol{u}_n^{hk}) - c(\rho_n^{hk}; \boldsymbol{u}_n^{hk}, \boldsymbol{u}_n - \boldsymbol{u}_n^{hk}) \geqslant C\|\boldsymbol{u}_n - \boldsymbol{u}_n^{hk}\|_V^2,
\end{aligned}
$$

and the regularity $\varphi \in C([0,T]; W^{1,\infty}(\Omega))$ (which implies that $\nabla\varphi_n \in [L^{\infty}(\Omega)]^d$), applying several times the inequality

$$
ab \leqslant \epsilon a^2 + \frac{1}{4\epsilon}b^2, \quad a, b, \epsilon \in \mathbb{R},\ \epsilon > 0,
$$

it leads to the following estimates for electric potential and displacement field, for all $\boldsymbol{v}^h \in V^h$ and $\psi^h \in W^h$,

$$
\begin{aligned}
&\|\boldsymbol{u}_n - \boldsymbol{u}_n^{hk}\|_V^2 + \|\varphi_n - \varphi_n^{hk}\|_W^2 \\
&\quad \leqslant C\left(\|\boldsymbol{u}_n - \boldsymbol{v}^h\|_V^2 + \|\rho_n - \rho_n^{hk}\|_Y^2 + \|\varphi_n - \psi^h\|_W^2\right).
\end{aligned}
\tag{3.13}
$$

Combining now estimates (3.11) and (3.13) we have the following estimates for numerical errors:

$$
\begin{aligned}
&\|\boldsymbol{u}_n - \boldsymbol{u}_n^{hk}\|_V^2 + \|\rho_n - \rho_n^{hk}\|_Y^2 + \|\varphi_n - \varphi_n^{hk}\|_W^2 \\
&\quad \leqslant Ck\sum_{j=1}^{n}\Big\{\|\boldsymbol{u}_j - \boldsymbol{u}_j^{hk}\|_V^2 + \|\varphi_j - \varphi_j^{hk}\|_W^2 + \|\rho_j - \rho_j^{hk}\|_Y^2 \\
&\qquad + \left\|\Phi_j - \frac{\rho_j - \rho_{j-1}}{k}\right\|_Y \|\rho_j - \xi_j^h\|_Y + \|\rho_j - \rho_{j-1}\|_Y^2 + \|\boldsymbol{u}_j - \boldsymbol{u}_{j-1}\|_V^2 \\
&\qquad + \|\varphi_j - \varphi_{j-1}\|_W^2 + \|\rho_j - \xi_j^h\|_Y^2 + \left\|\frac{\rho_j - \rho_{j-1}}{k} - \dot{\rho}_j\right\|_Y^2\Big\} + C\|\boldsymbol{u}_n - \boldsymbol{v}_n^h\|_V^2 \\
&\qquad + \frac{C}{k}\sum_{j=1}^{n-1}\|\rho_j - \xi_j^h - (\rho_{j+1} - \xi_{j+1}^h)\|_Y^2 + C\|\rho_1 - \xi_1^h\|_Y^2 + C\|\rho_n - \xi_n^h\|_Y^2 \\
&\qquad + C\|\varphi_n - \psi_n^h\|_W^2 + C\|\rho_0 - \rho_0^{hk}\|_Y^2 + C\|\boldsymbol{u}_0 - \boldsymbol{u}_0^{hk}\|_V^2 + C\|\varphi_0 - \varphi_0^{hk}\|_W^2
\end{aligned}
$$

for all $\{\xi_j^h\}_{j=1}^n \subset K^h$, $\boldsymbol{v}_n^h \in V^h$ and $\psi_n^h \in W^h$.

Keeping in mind the regularities $\boldsymbol{u} \in C^1([0,T]; V)$, $\varphi \in C^1([0,T]; W)$ and $\rho \in C^1([0,T]; Y)$ we easily find that

$$
k\sum_{j=1}^{n}\left\{\|\rho_j - \rho_{j-1}\|_Y^2 + \|\varphi_j - \varphi_{j-1}\|_W^2 + \|\boldsymbol{u}_j - \boldsymbol{u}_{j-1}\|_V^2\right\} \leqslant Ck^2.
$$

Finally, using a discrete version of Gronwall's inequality (see [20] for details), we obtain the following.

Theorem 3.1 *Let assumptions (i)–(iv) hold and assume that Problem VP has a unique solution* $(\boldsymbol{u}, \varphi, \rho)$ *with additional regularity (3.10). Let* $(\boldsymbol{u}^{hk}, \varphi^{hk}, \rho^{hk})$ *be the unique solution to Problem* VP^{hk}. *Then, there exists a positive constant* $C > 0$, *independent of the discretisation*

https://doi.org/10.1017/S0956792512000150 Published online by Cambridge University Press

parameters h and k but depending on the continuous solution $(\boldsymbol{u}, \varphi, \rho)$ and the problem data, such that, for all $\{\boldsymbol{v}_n^h\}_{n=0}^N \subset V^h$, $\{\psi_n^h\}_{n=0}^N \subset W^h$ and $\{\xi_n^h\}_{n=0}^N \subset K^h$,

$$\begin{aligned}\max_{0\leqslant n\leqslant N}\left\{\|\boldsymbol{u}_n-\boldsymbol{u}_n^{hk}\|_V^2+\|\varphi_n-\varphi_n^{hk}\|_W^2+\|\rho_n-\rho_n^{hk}\|_Y^2\right\}\leqslant C\Bigg(k\sum_{j=1}^{N}\Bigg\{\|\rho_j-\xi_j^h\|_Y^2\\ +\left\|\frac{\rho_j-\rho_{j-1}}{k}-\dot\rho_j\right\|_Y^2+\left\|\Phi_j-\frac{\rho_j-\rho_{j-1}}{k}\right\|_Y\|\rho_j-\xi_j^h\|_Y\Bigg\}+\|\varphi_0-\varphi_0^{hk}\|_W^2\\ +\max_{0\leqslant n\leqslant N}\|\rho_n-\xi_n^h\|_Y^2+\max_{0\leqslant n\leqslant N}\|\boldsymbol{u}_n-\boldsymbol{v}_n^h\|_V^2+\|\boldsymbol{u}_0-\boldsymbol{u}_0^{hk}\|_V^2+\|\rho_0-\rho_0^h\|_Y^2\\ +k^2+\max_{0\leqslant n\leqslant N}\left\|\varphi_n-\psi_n^h\right\|_W^2+\frac{1}{k}\sum_{j=1}^{N-1}\left\|\rho_j-\xi_j^h-(\rho_{j+1}-\xi_{j+1}^h)\right\|_Y^2\Bigg).\end{aligned}\tag{3.14}$$

The above error estimates are the basis for the analysis of the convergence rate of the algorithm. As an example, we can prove its linear convergence under some additional regularity conditions.

Corollary 1 *Let the assumptions of Theorem 3.1 still hold and let $\rho_0^{hk}=\mathscr{P}^h\rho_0$ be the initial discrete apparent density, where $\mathscr{P}^h$ is the $L^2(\Omega)$-projection operator onto B^h (see [8]). If we also assume that*

$$\begin{aligned}&\boldsymbol{u}\in L^\infty(0,T;[H^2(\Omega)]^d),\quad \varphi\in L^\infty(0,T;H^2(\Omega)),\\ &\rho\in H^2(0,T;Y)\cap H^1([0,T];H^1(\Omega))\cap C([0,T];H^2(\Omega)),\end{aligned}$$

then the algorithm is linearly convergent; that is, there exists a positive constant $C>0$, independent of the discretisation parameters h and k, such that

$$\max_{0\leqslant n\leqslant N}\left\{\|\boldsymbol{u}_n-\boldsymbol{u}_n^{hk}\|_V+\|\varphi_n-\varphi_n^{hk}\|_W+\|\rho_n-\rho_n^{hk}\|_Y\right\}\leqslant C(h+k).\tag{3.15}$$

The proof of this corollary is done as follows. First, we have (see [8]),

$$\begin{aligned}&\inf_{v_n^h\in V^h}\|\boldsymbol{u}_n-\boldsymbol{v}_n^h\|_V\leqslant Ch\|\boldsymbol{u}_n\|_{[H^2(\Omega)]^d}\leqslant Ch\|\boldsymbol{u}\|_{C([0,T];[H^2(\Omega)]^d)},\\ &\inf_{\psi_n^h\in W^h}\|\varphi_n-\psi_n^h\|_W\leqslant Ch\|\varphi_n\|_{H^2(\Omega)}\leqslant Ch\|\varphi\|_{C([0,T];H^2(\Omega))},\\ &\inf_{\xi_n^h\in K^h}\|\rho_n-\xi_n^h\|_Y\leqslant Ch\|\rho_n\|_{H^1(\Omega)}\leqslant Ch\|\rho\|_{C([0,T];H^1(\Omega))},\\ &\|\rho_0-\rho_0^{hk}\|_Y\leqslant Ch\|\rho_0\|_{H^1(\Omega)}\leqslant Ch\|\rho\|_{C([0,T];H^1(\Omega))}.\end{aligned}$$

Now applying estimates (3.13) for $n=0$ it follows that

$$\begin{aligned}&\|\boldsymbol{u}_0-\boldsymbol{u}_0^{hk}\|_V^2+\|\varphi_0-\varphi_0^{hk}\|_W^2\\ &\quad\leqslant C\left(\|\boldsymbol{u}_0-\boldsymbol{v}^h\|_V^2+\|\rho_0-\rho_0^{hk}\|_Y^2+\|\varphi_0-\psi^h\|_W^2\right),\end{aligned}$$

https://doi.org/10.1017/S0956792512000150 Published online by Cambridge University Press

for all $\boldsymbol{v}^h \in V^h$ and $\psi^h \in W^h$, and the above estimates imply that

$$\|\boldsymbol{u}_0 - \boldsymbol{u}_0^{hk}\|_V^2 + \|\varphi_0 - \varphi_0^{hk}\|_W^2 \leqslant Ch^2\Big(\|\rho\|^2_{C([0,T];H^1(\Omega))} + \|\boldsymbol{u}\|^2_{C([0,T];[H^2(\Omega)]^d)} + \|\varphi\|^2_{C([0,T];H^2(\Omega))}\Big).$$

It is easy to prove that

$$k\sum_{j=1}^N \left\|\frac{\rho_j - \rho_{j-1}}{k} - \dot\rho_j\right\|_Y^2 \leqslant Ck^2\|\rho\|^2_{H^2(0,T;Y)},$$

$$\begin{aligned} k\sum_{j=1}^N \left\|\Phi_j - \frac{\rho_j - \rho_{j-1}}{k}\right\|_Y \|\rho_j - \xi_j^h\|_Y &\leqslant k\sum_{j=1}^N \Big\{\|\Phi_j - \dot\rho_j\|_Y \|\rho_j - \xi_j^h\|_Y \\ &\quad + \left\|\dot\rho_j - \frac{\rho_j - \rho_{j-1}}{k}\right\|_Y \|\rho_j - \xi_j^h\|_Y\Big\} \\ &\leqslant C\max_{1\leqslant j\leqslant N}\|\rho_j - \xi_j^h\|_Y + C\sum_{j=1}^N k\Big\{\left\|\dot\rho_j - \frac{\rho_j - \rho_{j-1}}{k}\right\|_Y^2 + \|\rho_j - \xi_j^h\|_Y^2\Big\}. \end{aligned}$$

Finally, taking into account that (see [4]):

$$\frac{1}{k}\sum_{n=1}^{N-1}\|\rho_n - \xi_n^h - (\rho_{n+1} - \xi_{n+1}^h)\|_Y^2 \leqslant Ch^2\|\rho\|^2_{H^1(0,T;H^1(\Omega))},$$

$$\inf_{\xi_j^h \in K^h}\|\rho_j - \xi_j^h\|_Y \leqslant Ch^2\|\rho_j\|_{H^2(\Omega)} \leqslant Ch^2\|\rho\|_{C([0,T];H^2(\Omega))},$$

the previous estimates and Theorem 3.1 imply (3.15).

4 Numerical results

We now describe briefly the numerical scheme provided in Problem VP^{hk} and show some 1D and 2D numerical examples to demonstrate the accuracy of the algorithm and the behaviour of the solution.

4.1 Numerical scheme

First, we recall that variational spaces V, Q, W and B and convex set K are approximated using the finite element spaces V^h, Q^h, W^h and B^h, and the discrete convex set K^h, defined by (3.1), (3.2), (3.3), (3.4) and (3.5), respectively.

The discrete initial apparent density ρ_0^{hk} is given in (3.6) and (3.7) for $n = 0$, and, for $n = 1, 2, \ldots, N$, ρ_n^{hk} is known. Therefore, the discrete displacement field $\boldsymbol{u}_n^{hk}$ and the discrete electric potential φ_n^{hk} are found solving these coupled discrete linear variational equations:

$$\begin{aligned} &\boldsymbol{u}_n^{hk} \in V^h, \quad c(\rho_n^{hk}; \boldsymbol{u}_n^{hk}, \boldsymbol{v}^h) = (\boldsymbol{f}_n, \boldsymbol{v}^h)_V - ((\rho_n^{hk})^\gamma \mathscr{E}^* \nabla\varphi_n^{hk}, \boldsymbol{\varepsilon}(\boldsymbol{v}^h))_Q \ \ \forall \boldsymbol{v}^h \in V^h, \\ &\varphi_n^{hk} \in W^h, \quad ((\rho_n^{hk})^\gamma[\beta\nabla\varphi_n^{hk} - \mathscr{E}\boldsymbol{\varepsilon}(\boldsymbol{u}_n^{hk})], \nabla\psi^h)_H = (q_n, \psi^h)_W \ \ \forall \psi^h \in W^h. \end{aligned}$$

This is a linear problem which leads to a linear asymmetric system. The well-known LU method is employed for its resolution.

https://doi.org/10.1017/S0956792512000150 Published online by Cambridge University Press

Moreover, the discrete stress field is calculated from the equation,

$$\boldsymbol{\sigma}_n^{hk} = 2\,\mu(\rho_n^{hk})\boldsymbol{\varepsilon}(\boldsymbol{u}_n^{hk}) + \lambda(\rho_n^{hk})\mathrm{Div}\,(\boldsymbol{u}_n^{hk})\mathscr{I} + (\rho_n^{hk})^{\gamma}\mathscr{E}^{*}\nabla\varphi_n^{hk}.$$

Finally, for each $n = 1, 2, \ldots, N$ in the discrete variational inequality (3.8), since $\boldsymbol{u}_{n-1}^{hk}$, $\boldsymbol{\sigma}_{n-1}^{hk}$ and ρ_{n-1}^{hk} are known, it follows that the discrete apparent density function ρ_n^{hk} is the solution to

$$\begin{aligned}\rho_n^{hk} \in K^h, \quad \left(\rho_n^{hk}, \xi^h - \rho_n^{hk}\right)_Y &\geqslant k\left(\Phi(\rho_{n-1}^{hk}, \boldsymbol{\sigma}_{n-1}^{hk}, \boldsymbol{\varepsilon}(\boldsymbol{u}_{n-1}^{hk})), \xi^h - \rho_n^{hk}\right)_Y \\ &+ \left(\rho_{n-1}^{hk}, \xi^h - \rho_n^{hk}\right)_Y \quad \forall \xi^h \in K^h,\end{aligned}$$

which is solved by using a penalty-duality algorithm (see, e.g., [11]).

We note that the numerical scheme was implemented on a 3.2-Ghz PC using MATLAB, and a typical 1D run ($h = k = 0.001$) took about 4 minutes of CPU time and a run for the 2D example spent about 8 seconds for each time iteration.

4.2 Numerical convergence in a 1D example

In order to show the accuracy of the algorithm, the following 1D problem is considered.

Problem 1D Find the displacement field $u : [0,1] \times [0,1] \to \mathbb{R}$, the electric potential field $\varphi : [0,1] \times [0,1] \to \mathbb{R}$ and the apparent density function $\rho : [0,1] \times [0,1] \to [0.01, 1.74]$ such that

$$\begin{aligned}
&-\frac{\partial \sigma}{\partial x}(x,t) = 0 \quad x \in (0,1),\ t \in (0,1),\\
&-\frac{\partial D}{\partial x}(x,t) = 0 \quad x \in (0,1),\ t \in (0,1),\\
&\dot{\rho}(x,t) = \left(\frac{\sigma(x,t)\frac{\partial u}{\partial x}(x,t)}{2\rho(x,t)} - 0.004\right) \quad x \in [0,1],\ t \in [0,1],\\
&u(0,t) = 0 \quad t \in (0,1),\\
&\varphi(0,t) = 0 \quad t \in (0,1),\\
&\sigma(1,t) = -0.0001\, e^{t} \quad t \in (0,1),\\
&\rho(x,0) = 0.8 \quad x \in [0,1],
\end{aligned}$$

where the stress field $\sigma : [0,1] \times [0,1] \to \mathbb{R}$ and the electric displacement field D: $[0,1] \times [0,1] \to \mathbb{R}$ are given by, for all $x \in (0,1)$ and $t \in (0,1)$,

$$\begin{aligned}
\sigma(x,t) &= 3,790(\rho(x,t))^3\frac{\partial u}{\partial x}(x,t) + 2 \times 10^{-9}(\rho(x,t))^3\frac{\partial \varphi}{\partial x}(x,t),\\
D(x,t) &= 2 \times 10^{-9}(\rho(x,t))^3\frac{\partial u}{\partial x}(x,t) - 190 \times 10^{-15}(\rho(x,t))^3\frac{\partial \varphi}{\partial x}(x,t).
\end{aligned}$$

https://doi.org/10.1017/S0956792512000150 Published online by Cambridge University Press

Table 1. *Example 1D: numerical errors (×100) for some h and k*

$h \downarrow k \rightarrow$	0.1	0.05	0.01	0.005	0.001	0.0005	0.0001
0.0625			0.473426	0.473064	0.472774	0.472738	0.472709
0.03125	157.9005	76.30889	0.235741	0.235561	0.235416	0.235398	0.235383
0.015625	124.1726	0.117657	0.116933	0.116842	0.116771	0.116761	0.116754
0.0078125	0.058353	0.057899	0.057537	0.057492	0.057456	0.057451	0.057448
0.00390625	0.028249	0.028022	0.027841	0.027819	0.027801	0.027798	0.027797
0.001953125	0.013198	0.013084	0.012994	0.012983	0.012974	0.012972	0.012972
0.0009765625	0.005672	0.005615	0.005571	0.005565	0.005561	0.005559	0.005559

The above 1D problem corresponds to Problem P with the following data, keeping in mind that the area of the cross section is $A = 1\mathrm{m}^2$:

$$\Omega = (0,1), \quad T = 1\,\mathrm{day}, \quad E(\rho) = M\rho^{\gamma}, \quad M = 3790\,\mathrm{Nm}^2/\mathrm{kg}^2, \quad \gamma = 3,$$
$$B = 1, \quad \rho_a = 0.01\,\mathrm{kg/m}, \quad \rho_b = 1.740\,\mathrm{kg/m}, \quad S_r = 0.004\,\mathrm{kg/(ms)},$$
$$\rho_0 = 0.8\,\mathrm{kg/m}, \quad f = 0, \quad g(t) = -10^{-4}e^t\,\mathrm{N} \quad \text{for} \quad t \in [0,1].$$

In this example the numerical convergence of the algorithm is depicted. Several uniform partitions of both the time interval and the domain, dividing $\Omega = (0,1)$ into n segments, have been performed. Therefore, the spatial discretisation parameter h equals to $\frac{1}{n}$, and we used the solution obtained with $n = 2^{12}$ and $k = 10^{-4}$ as the 'exact solution'.

In Table 1 we show the numerical errors, multiplied by 100 and obtained for different discretisation parameters h and k, and given by

$$E^{hk} = \max_{0 \leqslant n \leqslant N} \left\{ \|\boldsymbol{u}_n - \boldsymbol{u}_n^{hk}\|_V + \|\rho_n - \rho_n^{hk}\|_Y + \|\varphi_n - \varphi_n^{hk}\|_W \right\}.$$

The convergence of the algorithm is clearly observed. Moreover, the evolution of the error depending on $h + k$ is plotted in Figure 2, from which we deduce that the linear convergence, stated in Corollary 1, seems to be achieved.

4.3 Numerical results for 2D problems

Here our aim is to first reproduce the simulation described in [49] considering the piezoelectric effects. This simulation aims to represent the daily load history using three loading cases acting sequentially, which corresponds to the walking activity. Each load consists in one compressive load acting on the femoral head plus the reaction force induced in the abductor muscle. Now we will obtain electrical effects because of the mechanical loads that are acting on the bone. In order to avoid the lack of connection between the cortical layers of the diaphysis, we include a side plate joining both layers (see [6, 23]). We assume that the lower horizontal boundary is fixed through the vertical direction, whereas the left point is clamped. Moreover, at this point the potential field is equal to zero. Finally, we consider a plain strain hypothesis in which the proximal femur has a uniform thickness of 10 mm and the side plate 1 mm.

https://doi.org/10.1017/S0956792512000150 Published online by Cambridge University Press

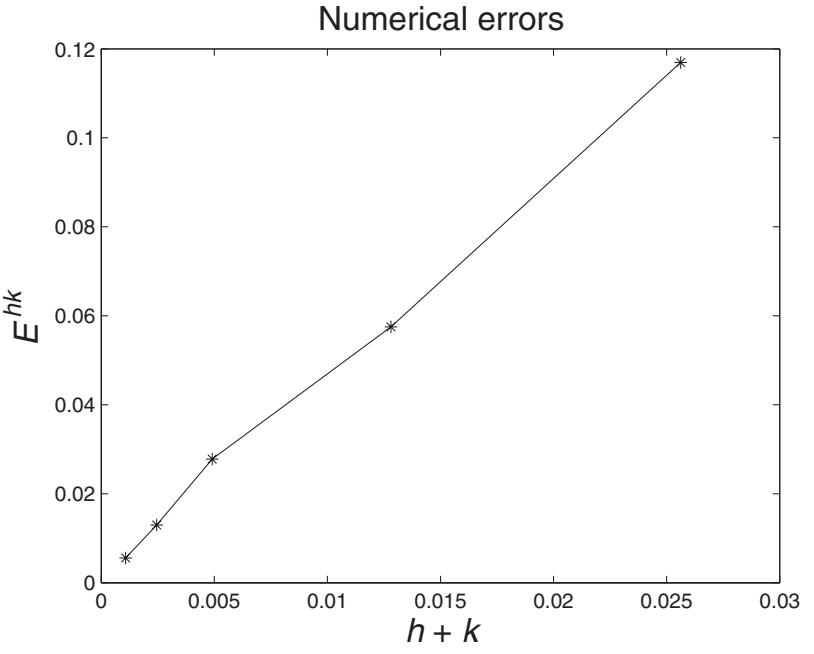


FIGURE 2. Example 1D: Asymptotic constant error.

The following data have been used in this simulation:

$$T = 300\,\text{days}, \quad E(\rho) = M\rho^{\gamma}, \quad M = 3,790\,\text{Pa}/(\text{kg m}^{-2})^2, \quad \gamma = 3,$$
$$\boldsymbol{f} = \mathbf{0}\,\text{N/m}^2, \quad B = 1\,(\text{g cm}^{-3})^2(\text{MPa day})^{-1}, \quad S_r = 0.004\ \text{J/g},$$
$$\kappa = 0.3, \quad \rho_a = 0.01\,\text{g/cm}^3, \quad \rho_b = 1.740\,\text{g/cm}^3, \quad \rho_0 = 0.8\,\text{g/cm}^3,$$
$$\beta_{11} = 88.54 \times 10^{-12}\,\text{F/mm}, \quad \beta_{33} = 106.248 \times 10^{-12}\,\text{F/mm},$$
$$e_{31} = 1.50765 \times 10^{-9}\,\text{C/mm}^2, \quad e_{33} = 1.87209 \times 10^{-9}\,\text{C/mm}^2,$$
$$e_{15} = 3.57643 \times 10^{-9}\,\text{C/mm}^2.$$

In Figure 3 we observe the configuration of bone density after 300 days. The end configuration predicts a reasonably accurate density distribution with an intramedullary canal. As it was also noted in [49], Ward's triangle and the typical cancellous density patterns in this femoral head are shown. Comparing these results with those obtained in [11] for the model without piezoelectricity, we can observe that, in this example, the electrical field does not have an important influence on the distribution of bone density, maybe because the potential field generated by these mechanical loads is small. In Figure 4 the electric potential is plotted at different instants of the 215th day. We can observe several variations in the distribution of electric charges and its values, caused by the application of different mechanical loads.

Then we will assume that between days 300 and 400 the physical activity is reduced and the mechanical loads are applied only on one of each three days. As we observe in Figure 5, the bone density in the femoral head at time $t = 400$ days is lower than at $t = 300$ days.

Probably, the most important advantage of considering piezoelectric effects in bone remodelling is the ability to change bone density by applying electric charges. When we

https://doi.org/10.1017/S0956792512000150 Published online by Cambridge University Press

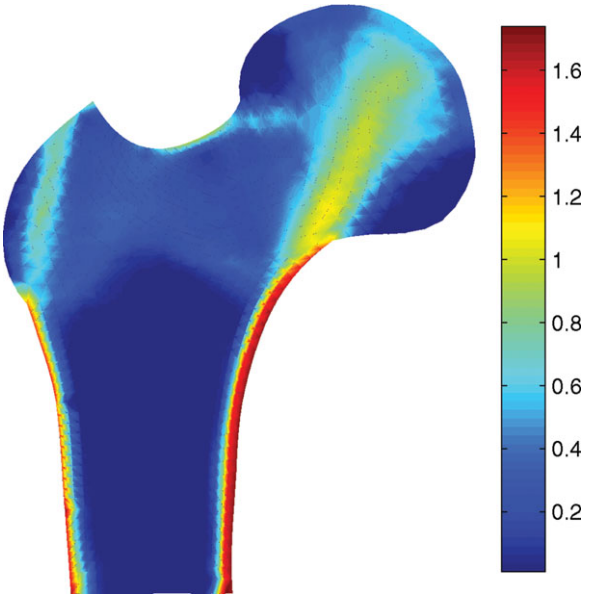


FIGURE 3. (Colour online) Bone density after 300 days.

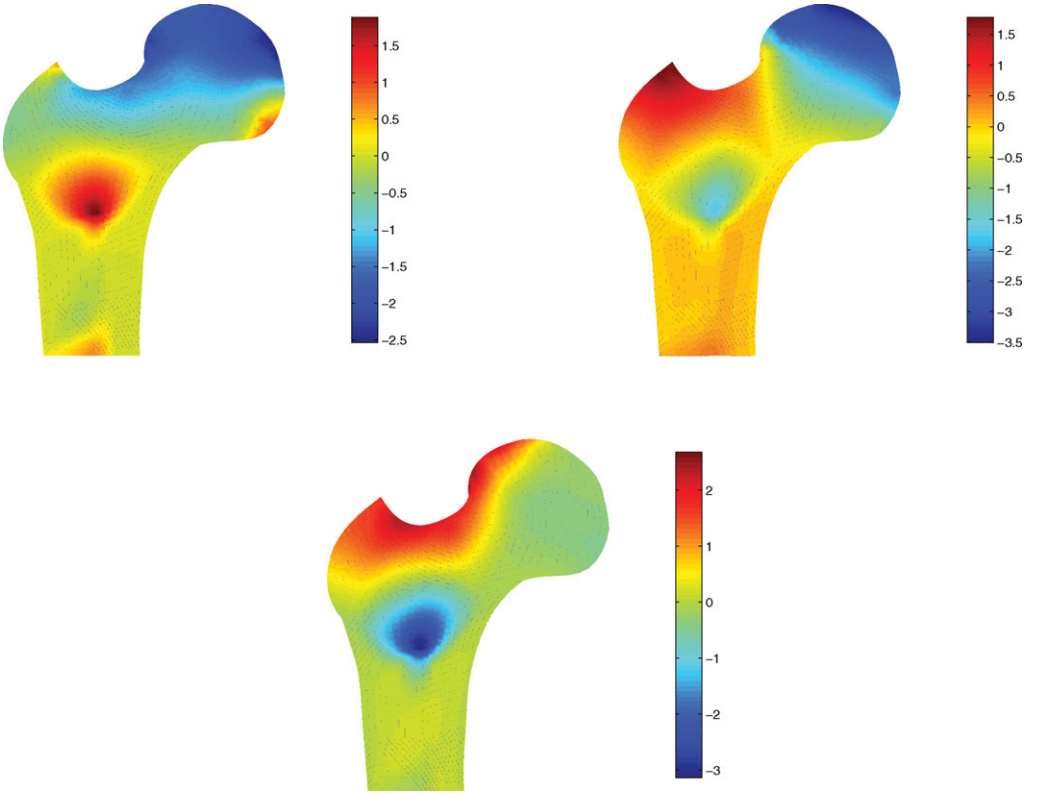


FIGURE 4. (Colour online) The potential field at several times ($t = 215$, 215.2 and 215.4).

https://doi.org/10.1017/S0956792512000150 Published online by Cambridge University Press

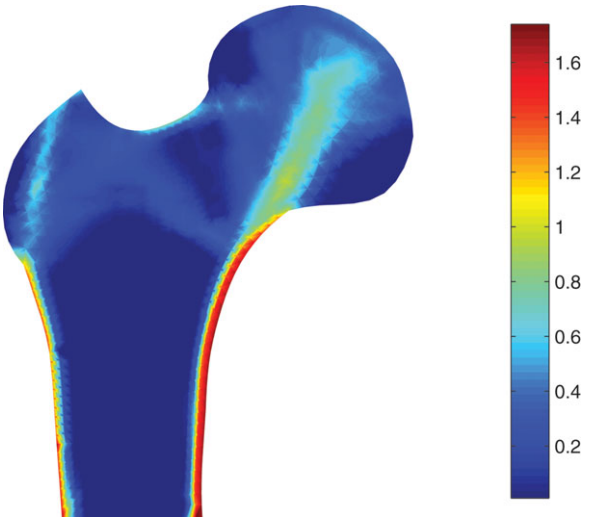


FIGURE 5. (Colour online) Bone density after a period of reduced physical activity ($t = 400$ days).

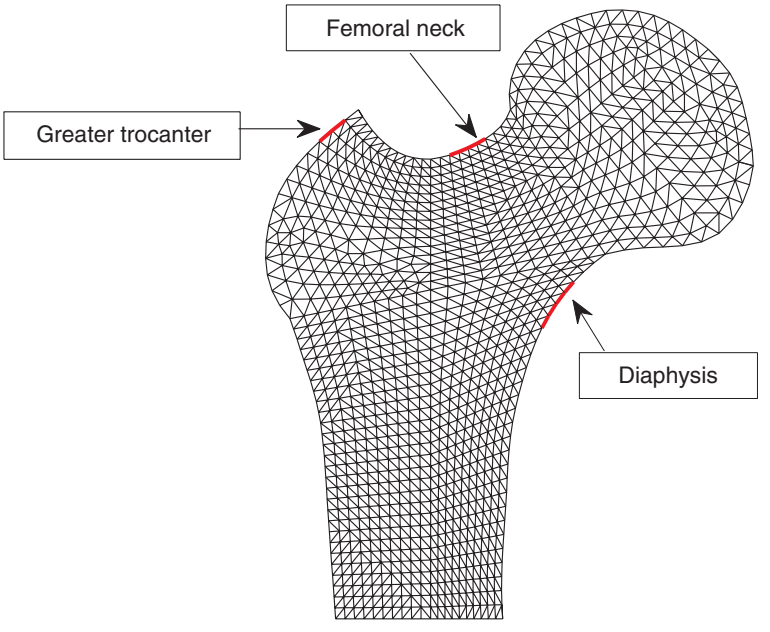


FIGURE 6. (Colour online) Boundaries for electric charge.

apply an electric charge in a piezoelectric material, we obtain an associated mechanical displacement and, for a bone, we obtain a change in bone density. In the following simulations we will try to show how an electrical charge can change the bone density distribution. Then we will assume the configuration obtained after 300 days and will consider that an electric charge is applied on three different parts of the bone during a period of reduced physical activity (see Figure 6). Moreover, we will compare the bone

https://doi.org/10.1017/S0956792512000150 Published online by Cambridge University Press

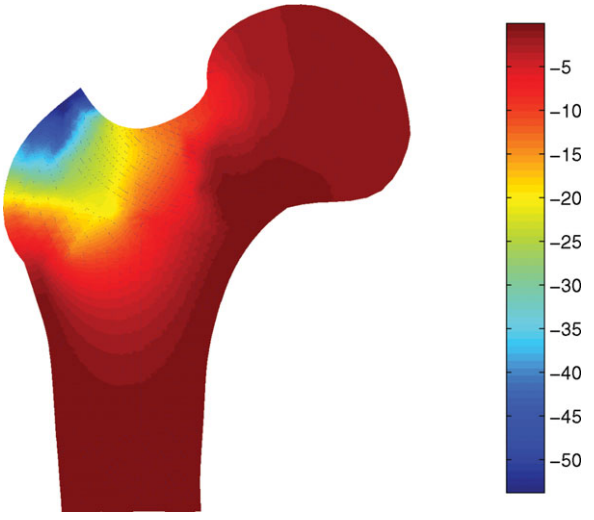


FIGURE 7. (Colour online) Electric potential after a period of reduced physical activity ($t = 400$ days) in which an electric charge is acting on the greater trocanter.

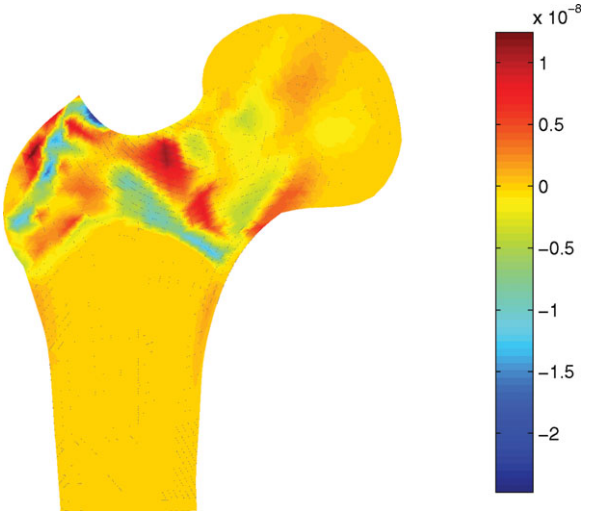


FIGURE 8. (Colour online) Differences between bone density when an electric charge is applied and when only mechanical loads are acting ($t = 400$ days).

density corresponding to each case with the previously obtained bone density when no electrical forces were applied (see Figure 5).

An electric charge on the greater trocanter. In this first case, an electric load is applied on the greater trocanter (see Figure 6) between days 300 and 400. During this time, the mechanical loads are applied only on one of each three days. Applying the electrical surface charge of $2 \times 10^{-9}\,\mathrm{C/mm^2}$ we obtain a negative potential field with a maximum intensity of $-50\,\mathrm{V}$ (see Figure 7). In order to show the variation of bone density, we plot in Figure 8 the differences between bone density, when an electric charge is applied and when only mechanical loads are acting. In spite of the small differences obtained,

https://doi.org/10.1017/S0956792512000150 Published online by Cambridge University Press

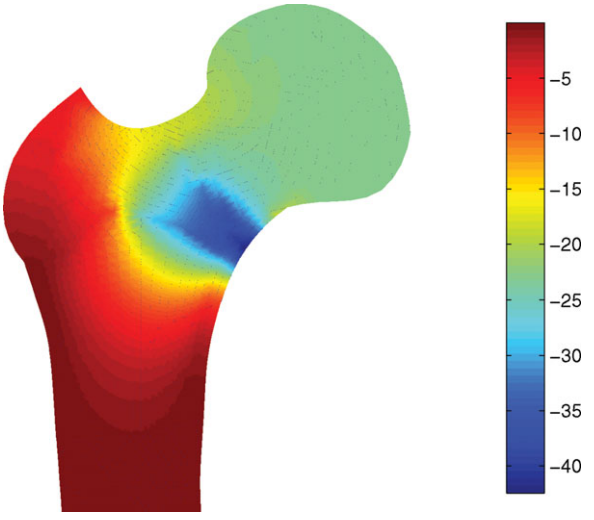


FIGURE 9. (Colour online) Electric potential after a period of reduced physical activity ($t = 400$ days) in which an electric charge is acting on the diaphysis.

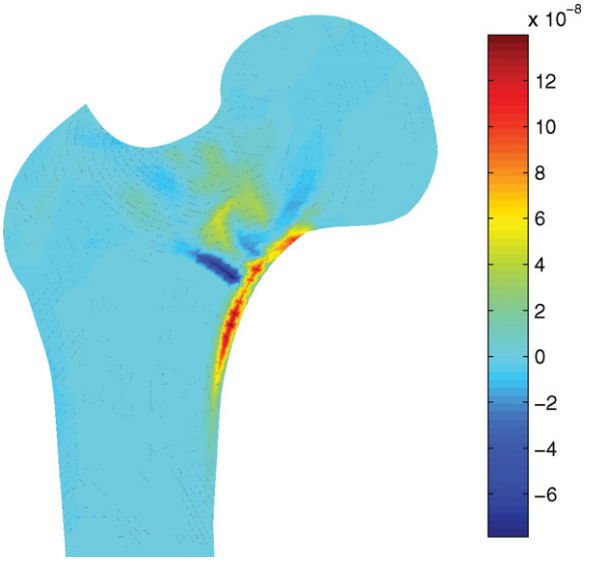


FIGURE 10. (Colour online) Differences between bone density when an electric charge is applied and when only the mechanical loads are acting ($t = 400$ days).

we observe that in the areas in red an increment in the bone density has been produced. However, in the areas in blue the bone density has decreased when the electric charge was applied.

An electric charge on the diaphysis. In the second example we apply an electric load on the upper part of the diaphysis (see Figure 6). In this case an electrical surface charge of $5 \times 10^{-8}\,\mathrm{C/mm^2}$ is applied. In Figure 9 we see that the electric charge produces a potential field with a maximum intensity of $-40\,\mathrm{V}$.

https://doi.org/10.1017/S0956792512000150 Published online by Cambridge University Press

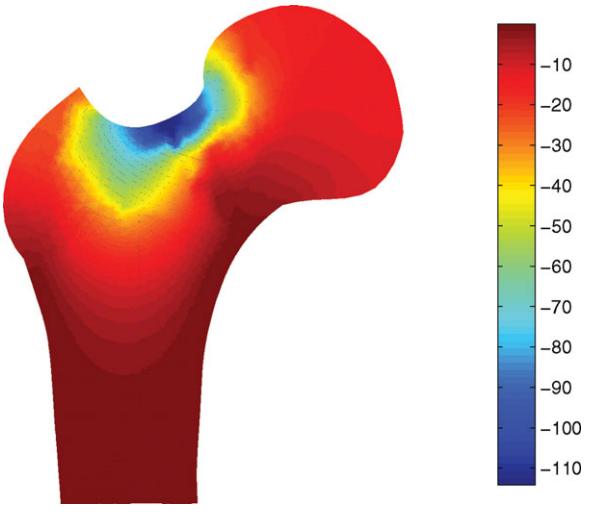


FIGURE 11. (Colour online) Electric potential after a period of reduced physical activity ($t = 400$ days) in which an electric charge is applied.

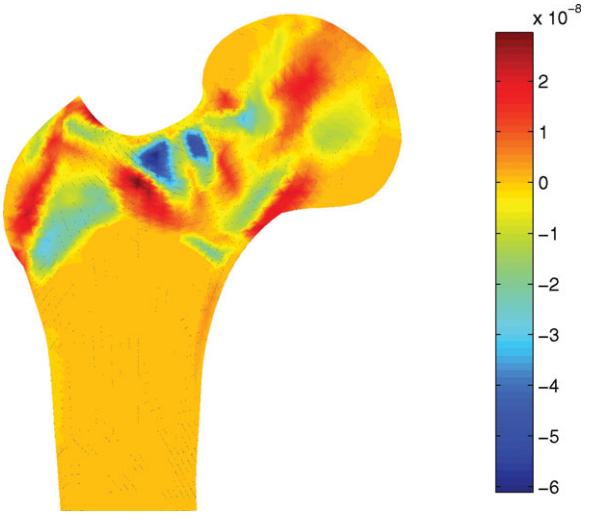


FIGURE 12. (Colour online) Differences between bone density when an electric charge is applied and when only the mechanical loads are acting ($t = 400$ days).

The differences between bone density, when only the mechanical loads are acting and when an electric charge is applied, are plotted in Figure 10. In this case, the electric charge mainly affects the closer area of the application point, producing an increase in bone density near the cortical bone.

An electric charge on the femoral neck. As a final example, we consider an electrical charge of $2 \times 10^{-9}\,\mathrm{C/mm^2}$ acting on the upper part of the femoral neck (see Figure 6). The potential field at 400 days is plotted in Figure 11. In this case, the porosity decreases in several areas, remarking those areas with higher density (see Figure 12).

https://doi.org/10.1017/S0956792512000150 Published online by Cambridge University Press

5 Conclusions

A piezoelectric strain-adaptive bone remodelling problem was numerically studied in this paper. Fully discrete approximations were introduced by using the finite element method to approximate the spatial variable and an Euler scheme to discretise time derivatives. An *a priori* error estimates result was proved, Theorem 3.1, from which, under adequate additional regularity conditions, the linear convergence of the algorithm was derived (see Corollary 1).

The algorithm was implemented by using MATLAB code and some examples were computed. First, a simple 1D problem was chosen in such a way as to show the numerical convergence of the algorithm. As can be seen in Figure 2, the linear convergence of the algorithm was achieved. Then the simulation of a 2D proximal femur was performed. First, we compared the bone density distribution, influenced by the piezoelectric effects, in a normal daily activity and after its reduction. The results obtained demonstrated a reduction in bone density (see Figures 3 and 5). Then we assumed the application of a surface electric charge in three different areas, in order to compare the bone density distribution for each of them. We chose the greater trocanter, the diaphysis and the femoral neck. Differences between the results in each case and those obtained when only mechanical loads were applied were reported.

We remark that the purpose of this work was to present a piezoelectric formulation and simulation model of bone remodelling, which could be used in future to design electro-mechanical protocols in order to reduce bone loss under pathological conditions such as bone osteoporosis.

Finally, we notice that this work presents a computational approach that allows studying and understanding the effect of bone piezoelectricity on bone remodelling coupling influences of loading and electric field on bone response. Nevertheless, we have to keep in mind that this model is a first approach to the problem of bone piezoelectricity and additional effects should be included. The idea that bone matrix piezoelectricity acts in conjunction with streaming potential is commonly accepted in the literature, although the exact coupling mechanism between both phenomena is still unknown. Therefore, the future development of more complete multiphysics models that allow the modelling of multiple coupled phenomena (matrix piezoelectricity, streaming potentials and strain-generated fluid flow) would be very beneficial to advance the understanding of bone physiology.

References

[1] Ahn, A. C. & Grodzinsky A. J. (2009) Relevance of collagen piezoelectricity to "Wolff's Law": A critical review. *Med. Eng. Phys.* **31**(7), 733–741.

[2] Anderson, J. C. & Eriksson, C. (1968) Electrical properties of wet collagen. *Nature* **218**, 167–169.

[3] Anderson, J. C. & Eriksson, C. (1970) Piezoelectric properties of dry and wet bone. *Nature* **227**, 491–492.

[4] Barboteu, M., Fernández, J. R. & Hoarau-Mantel, T. V. (2005) A class of evolutionary variational inequalities with applications in viscoelasticity. *Math. Models Methods Appl. Sci.* **15**(10), 1595–1617.

https://doi.org/10.1017/S0956792512000150 Published online by Cambridge University Press

[5] Batra, R. C. & Yang, J. S. (1995) Saint-Venant's principle in linear piezoelectricity. *J. Elast.* **38**, 209–218.
[6] Beaupré, G. S., Orr, T. E. & Carter, D. R. (1990) An approach for time-dependent bone modeling and remodeling-theoretical development. *J. Orthop. Res.* **8**, 651–661.
[7] Becker, R. O. & Marino, A. A. (1982) *Electromagnetism and Life*, State University of New York Press, Albany, NY.
[8] Ciarlet, P. G. (1991) The finite element method for elliptic problems. In: P. G. Ciarlet and J. L. Lions (editors), *Handbook of Numerical Analysis*, Vol. 2, North Holland, Amsterdam, Netherlands, pp. 17–352.
[9] Cowin, S. C. (2006) The exact stimulus of the strain adaptation of bone tissue is unknown. *J. Biomech. Sci. Eng.* **1**(1), 16–28.
[10] Cowin, S. C. & Hegedus, D. H. (1976) Bone remodeling I: Theory of adaptive elasticity. *J. Elast.* **6**(3), 313–326.
[11] Fernández, J. R., García-Aznar, J. M., Martínez, R. & Viaño, J. M. (2010) Numerical analysis of a strain-adaptive bone remodelling problem. *Comput. Methods Appl. Mech. Eng.* **199**, 1549–1557.
[12] Fernández, J. R. & Kuttler, K. L. (2009) An existence and uniqueness result for an elasto-piezoelectric problem with damage. *Math. Models Methods Appl. Sci.* **19**(1), 31–50.
[13] Fotiadis, D. I., Foutsitzi, G. & Massalas, C. V. (2000) Wave propagation in human long bones of arbitrary cross-section. *Int. J. Eng. Sci.* **38**, 1553–1591.
[14] Frost, H. M. (1987) Vital biomechanics. Proposed general concepts for skeletal adaptations to mechanical usage. *Calcif. Tissue Int.* **42**, 145–156.
[15] Fukada, E. & Yasuda, I. (1957) On the piezoelectric effect of bone. *J. Phys. Soc. Japan* **12**, 1158–1162.
[16] Fukada, E. & Yasuda, I. (1964) Piezoelectric effects in collagen. *Japan J. Appl. Phys.* **3**, 117–121.
[17] Gjelsvik, A. (1973) Bone remodelling and piezoelectricity II. *J. Biomech.* **6**, 187–193.
[18] Glowinski, R. (1984) *Numerical Methods for Nonlinear Variational Problems*, Springer-Verlag, New York.
[19] Guzelsu, N. (1978) A piezoelectric model for dry bone tissue. *J. Biomech.* **11**, 257–267.
[20] Han, W. & Sofonea, M. (2002) *Quasistatic Contact Problems in Viscoelasticity and Viscoplasticity*, American Mathematical Society International Press, Berkeley, CA.
[21] Hegedus, D. H. & Cowin, S. C. (1976) Bone remodeling II: Small strain adaptive elasticity. *J. Elast.* **6**(4), 337–352.
[22] Huiskes, R., Weinans, H. & Dalstra, M. (1989) Adaptive bone remodeling and biomechanical design considerations for noncemented total hip arthroplasty. *Orthopedics* **12**, 1255–1267.
[23] Huiskes, R., Weinans, H., Grootenboer, H. J., Dalstra, M., Fudala, B. & Sloof, T. J. (1987) Adaptive bone-remodeling theory applied to prosthetic-design analysis. *J. Biomech.* **20**, 1135–1150.
[24] Huiskes, R., Weinans, H., Summer, D. R., Fudala, B., Turner, T. M., Grootenboer, H. J. & Galante, J. (1989) Stress-shielding, stress-bypassing and bone resorption around "press-fit" and bone ingrowth THA. *Trans. 35th Ann. Meeting Orthop. Res. Soc.* **14**, 529.
[25] Ideka, T. (1990) *Fundamentals of Piezoelectricity*, Oxford University Press, Oxford, UK.
[26] Isaacson, B. M. & Bloebaum, R. D. (2010) Bone bioelectricity: What have we learned in the past 160 years? *J. Biomed. Mater. Res.* A **95**(4), 1270–1279.
[27] Kirchner, H. O. K. & Lazar, M. (2008) The thermodynamic driving force for bone growth and remodelling: A hypothesis. *J. R. Soc. Interface* **5**, 183–193.
[28] Lakes, R. S. & Katz, J. L. (1977) Dielectric relaxation in cortical bone. *J. Appl. Phys.* **48**, 808–811.
[29] Martin, R. B., Burr, D. B. & Sharkey, N. A. (1998) *Skeletal Tissue Mechanics*, Springer, New York.

https://doi.org/10.1017/S0956792512000150 Published online by Cambridge University Press

[30] Migorski, S., Ochal, A. & Sofonea, M. (2009) Weak solvability of a piezoelectric contact problem. *Eur. J. Appl. Math.* **20**, 145–167.
[31] Migorski, S., Ochal, A. & Sofonea, M. (2010) Variational analysis of fully coupled electro-elastic frictional contact problem. *Math. Nachr.* **283**(9), 1314–1335.
[32] Migorski, S., Ochal, A. & Sofonea, M. (2011) Analysis of a quasistatic contact problem for piezoelectric materials. *J. Math. Anal. Appl.* **382**, 701–713.
[33] Mindlin, R. D. (1968) Polarisation gradient in elastic dielectrics. *Int. J. Solids Struct.* **4**, 637–663.
[34] Mindlin, R. D. (1969) Continuum and lattice theories of influence of electromechanical coupling on capacitance of thin dielectric films. *Int. J. Solids Struct.* **4**, 1197–1213.
[35] Mindlin, R. D. (1972) Elasticity, piezoelasticity and crystal lattice dynamics. *J. Elast.* **4**, 217–280.
[36] Morro, A. & Straughan, B. (1991) A uniqueness theorem in the dynamical theory of piezoelectricity. *Math. Methods Appl. Sci.* **14**(5), 295–299.
[37] Pollack, S. R. (2001) Streaming potentials in bone. In: S. C. Cowin (editors), *Bone Mechanics Handbook*, Taylor & Francis, Boca Raton, FL, pp. 24.1–24.17.
[38] Qin, Q. H. & Ye, J. Q. (2004) Thermoelectroelastic solutions for internal bone remodeling under axial and transverse loads. *Int. J. Solids Struct.* **41**, 2447–2460.
[39] Ramtani, S. (2008) Electro-mechanics of bone remodelling. *Int. J. Eng. Sci.* **46**, 1173–1182.
[40] Saha, S. & Williams, P. A. (1992) Electric and dieletric properties of wet human cortical bone as a function of frequency. *IEEE Trans. Biomed. Eng.* **39**(12), 1298–1304.
[41] Singh, S. & Saha, S. (1984) Electrical properties of bone. *Clin. Orthop. Relat. Res.* **186**, 249–271.
[42] Smit, T. H., Burguer, E. H. & Huyghe, J. M. (2002) A case for strain-induced fluid flow as a regulator of BMU-coupling and osteonal alignment. *J. Bone Mineral Res.* **17**(11), 2021–2029.
[43] Toupin, R. A. (1956) The elastic dielectrics. *J. Ration. Mech. Anal.* **5**, 849–915.
[44] Toupin, R. A. (1960) Stress tensors in elastic dielectrics. *Arch. Ration. Mech. Anal.* **5**, 440–452.
[45] Toupin, R. A. (1963) A dynamical theory of elastic dielectrics. *Int. J. Eng. Sci.* **1**, 101–126.
[46] Turbé, N. & Maugin, G. A. (1991) On the linear piezoelectricity of composite materials. *Math. Methods Appl. Sci.* **14**(6), 403–412.
[47] Wang, L., Fritton, S. P., Cowin, S. C. & Weinbaum, S. (1999) Fluid pressure relaxation depends upon osteonal microstructure: Modeling an oscillatory bending experiment. *J. Biomech.* **32**, 663–672.
[48] Weinans, H., Huiskes, R. & Grootenboer, H. J. (1989) Convergence and uniqueness of adaptive bone remodeling. *Trans. 35th Ann. Meeting Orthop. Res. Soc.* **14**, 310.
[49] Weinans, H., Huiskes, R. & Grootenboer, H. J. (1992) The behavior of adaptive bone-remodeling simulation models. *J. Biomech.* **25**(12), 1425–1441.
[50] Xinhua, Y., Chuanyao, C., Yuantai, H. & Cheng, W. (2005) Combined damage fracture criteria for piezoelectric ceramics. *Acta Mech. Sin.* **18**(1), 21–27.
[51] Wolff, J. (1986) The Law of Bone Remodelling, Springer, Berlin.

https://doi.org/10.1017/S0956792512000150 Published online by Cambridge University Press